

Estimation of surface-layer scaling parameters in the unstable boundary layer: implications for orographic flow speed-up

Article

Accepted Version

Argain, J. L., Teixeira, M. ORCID: <https://orcid.org/0000-0003-1205-3233> and Miranda, P. M. A. (2017) Estimation of surface-layer scaling parameters in the unstable boundary layer: implications for orographic flow speed-up. *Boundary-Layer Meteorology*, 165 (1). pp. 145-160. ISSN 0006-8314 doi: <https://doi.org/10.1007/s10546-017-0260-3> Available at <https://centaur.reading.ac.uk/70672/>

It is advisable to refer to the publisher's version if you intend to cite from the work. See [Guidance on citing](#).

Published version at: <https://link.springer.com/article/10.1007/s10546-017-0260-3>

To link to this article DOI: <http://dx.doi.org/10.1007/s10546-017-0260-3>

Publisher: Springer

All outputs in CentAUR are protected by Intellectual Property Rights law, including copyright law. Copyright and IPR is retained by the creators or other copyright holders. Terms and conditions for use of this material are defined in the [End User Agreement](#).

www.reading.ac.uk/centaur

CentAUR

Central Archive at the University of Reading

Reading's research outputs online

[Click here to view linked References](#)

1 Estimation of surface-layer scaling parameters in the unstable 2 boundary-layer: implications for orographic flow speed-up

3

4 José Luís Argain • Miguel A. C. Teixeira • Pedro M. A. Miranda

5

6

7 Received: DD Month YEAR/ Accepted: DD Month YEAR

8 **Abstract** A method is proposed for estimating the surface-layer depth (z_s) and the
9 friction velocity (u_*) as a function of stability (here quantified by the Obukhov length, L)
10 over the complete range of unstable flow regimes. This method extends the one
11 developed previously by the authors for stable conditions in Argain et al. ([Boundary-
12 Layer Meteorol, 2009, Vol.130, 15-28](#)), but uses a qualitatively different approach. The
13 method is specifically used to calculate the fractional speed-up (ΔS) in flow over a ridge,
14 although it is suitable for more general boundary-layer applications. The behaviour of
15 $z_s(L)$ and $u_*(L)$ as a function of L is indirectly assessed via calculation of $\Delta S(L)$ using
16 the linear model of Hunt et al. ([Q J R Meteorol Soc, 1988, Vol.29, 16-26](#)) and its
17 comparison with the field measurements reported in Coppin et al. ([Boundary-Layer
18 Meteorol, 1994, Vol.69, 173-199](#)) and with numerical simulations carried out using a
19 nonlinear numerical model, FLEX. The behaviour of ΔS estimated from the linear model
20 is clearly improved when u_* is calculated using the method proposed here, confirming
21 the importance of accounting for the dependences of $z_s(L)$ and $u_*(L)$ on L to better
22 represent processes in the unstable boundary-layer.

23

José Luis Argain

Departamento de Física, FCT, Universidade do Algarve, Faro 8005-139, Portugal.

jargain@ualg.pt

Miguel Ângelo Cortez Teixeira

Department of Meteorology, University of Reading, Earley Gate, PO Box 243, Reading RG6 6BB, UK

m.a.teixeira@reading.ac.uk

Pedro Manuel Alberto de Miranda

Instituto Dom Luiz, Faculdade de Ciências, Universidade de Lisboa, Lisbon 1749-016, Portugal

pmmiranda@fc.ul.pt

24 **Keywords** Convective boundary layer · Flow speed-up · Friction velocity · Surface-layer
25 height · Unstable stratification

26

27 **1 Introduction**

28 Fractional speed-up (ΔS) of flow over hills or mountains is defined as the ratio of the
29 speed perturbation at a given height to the upstream, unperturbed flow speed at the same
30 height. This quantity is highly relevant both from meteorological and wind engineering
31 perspectives, since it characterizes the modulation of the wind speed by orography. [Hunt
32 et al. \(1988\)](#) (hereafter HLR) developed one of the first theoretical linear atmospheric
33 boundary layer (ABL) models of flow over hills, which is one of the simplest and
34 computationally cheapest tools available for estimating ΔS .

35 However, stratification affects ΔS and must be carefully accounted for in the evaluation
36 of the scaling parameters that characterize the ABL. Among these, a key parameter is the
37 friction velocity (u_*), and another one is the surface-layer depth (z_s), usually estimated as
38 5% to 10% of the ABL depth.

39 [Weng \(1997\)](#) (hereafter W97), after implementing a continuous wind profile in the HLR
40 model, found that his predictions of ΔS disagreed significantly with the observations of
41 [Coppin et al. \(1994\)](#) (hereafter C94). [Argaín et al. \(2009\)](#) (hereafter A09) showed that
42 these discrepancies were due to the fact that the calculations in W97 were carried out
43 assuming that u_* is constant, regardless of the different observed stability regimes. They
44 proposed a method for estimating u_* in stably-stratified flows, which has led to an
45 improved prediction of ΔS over 2D hills. C94 also compared their observations with
46 predictions from the HLR model, and found considerable disagreement, both in stable
47 and unstable conditions. Here we show that, as in stably-stratified flows, a decisive
48 reason for such disagreements in unstable flow is the assumption of constant u_* .

49 In the present study, a new method is developed for estimating z_s and u_* as a function of
50 stability (here quantified by the Obukhov length, L) over the complete unstable
51 stratification range, i.e. from the free-convection to the neutral stability limits. Procedures
52 are developed for estimating z_s in a neutral ABL, and for estimating this and several
53 other scaling parameters, such as u_* , L and Deardorff's convective velocity scale, w_* , in
54 the free-convection regime, which are preliminary steps for defining $z_s(L)$ and $u_*(L)$ for

55 all stabilities. Given that the physical processes taking place in the CBL and in an
56 unstable surface layer are substantially different from those in a stable boundary ABL,
57 the method used to represent them also differs substantially, requiring the use of
58 additional theory.

59 The main motivation for developing this new method for estimating $z_s(L)$ and $u_*(L)$ is
60 the calculation of $\Delta S(L)$ for unstable flow over hills, although it must be noted that the
61 method can also be used for more general boundary layer applications. The calculation of
62 $\Delta S(L)$ requires knowing $u_*(L)$ which, in the method proposed here, also requires
63 estimating $z_s(L)$. The behaviour of $z_s(L)$ and $u_*(L)$ is thus indirectly assessed through
64 the calculation of $\Delta S(L)$ using the HLR model. These predictions are compared with field
65 measurements, reported in C94, and numerical simulations, carried out using a 2D
66 microscale-mesoscale non-hydrostatic model, FLEX. These comparisons allow us to
67 show how $z_s(L)$ and $u_*(L)$ are sometimes not estimated in a physically consistent way, a
68 limitation that the present method aims to overcome.

69 Section 2 presents the method that accounts for unstable stratification in the ABL and its
70 calibration. Section 3 describes the main results, namely comparisons between theory,
71 numerical simulations and measurements, using the new unstable ABL formulation.
72 Finally, Sect. 4 summarizes the main conclusions of this study.

73

74 **2 Methodology**

75 2.1 Unstable ABL model

76 Several studies show that the ABL, under moderately to strongly unstable stratification
77 (usually known as CBL), can be represented by a simplified three-layer bulk model (e.g.,
78 Garratt 1992). This comprises a thin statically unstable surface layer of depth z_s , a well-
79 mixed layer, of height z_i and depth $\Delta z_i = z_i - z_s$, and a transition layer of thickness
80 Δz_{ci} , coinciding with a temperature inversion capping the mixed layer, which inhibits
81 vertical mixing. In the mixed layer, quantities such as the mean potential temperature (θ)
82 and wind velocity (U, V) are well-mixed, and therefore constant with height, i.e. $\theta(z) =$
83 $const.$, $U(z) = const.$ and $V(z) = 0$. For our purposes, the strict fulfilment of these
84 profile shapes in the mixed layer is not critical, since we are essentially interested in the
85 surface layer, for which typically $z_s \approx 0.05z_i$ to $0.1z_i$ (Stull 1988). In the surface layer we

86 assume that the turbulent shear stresses have much more important effects on the mean
 87 flow than the Coriolis force. Hence, the Coriolis parameter (f) is set to zero, except
 88 where otherwise explicitly stated. Since the surface layer has characteristics which make
 89 it markedly different from the mixed layer, z_s can be defined as an important length scale
 90 of the ABL, essential for describing the impact of the orography on the wind profile. This
 91 follows [McNaughton \(2004\)](#), who established z_s as a new basis parameter for similarity
 92 models of the surface layer. In the method proposed here, z_s is essential for estimating
 93 the key velocity scale, u_* , and hence for calculating $\Delta S(L)$.

94

95 2.2 Surface-layer model

96 According to Monin-Obukhov similarity theory (MOST), in the surface layer the non-
 97 dimensional vertical gradients of $U(z)$ and $\theta(z)$ are universal functions of the parameter
 98 z/L , taking the forms

$$99 \quad \Phi_m\left(\frac{z}{L}\right) = \frac{\kappa z}{u_*} \frac{\partial U}{\partial z}, \quad (1)$$

100 and

$$101 \quad \Phi_h\left(\frac{z}{L}\right) = \frac{\kappa z}{Pr_t \theta_*} \frac{\partial \theta}{\partial z}, \quad (2)$$

102 where z is the height above the effective ground level, κ is the von Kármán constant,
 103 Pr_t is the turbulent Prandtl number and θ_* represents the surface-layer scaling
 104 temperature. u_* and θ_* , are defined using the vertical eddy kinematic fluxes of
 105 momentum and heat at the surface, i.e. $u_*^2 = \overline{(w'u')}_0$ and $\theta_* = -\overline{(w'\theta')}_0/u_*$. The length
 106 L is given by

$$107 \quad L = -\frac{\theta_0 u_*^3 / \kappa}{g \overline{(w'\theta')}_0} = \frac{\theta_0 u_*^2}{g \kappa \theta_*}, \quad (3)$$

108 where θ_0 is the potential temperature at the surface and g is the gravitational
 109 acceleration. [Wilson \(2001\)](#) (hereafter W01), after analyzing several forms of the
 110 functions Φ_m and Φ_h , proposed the following general form for the unstable regime (z/L
 111 < 0),

112
$$\Phi = \left(1 + \gamma \left| \frac{z}{L} \right|^{\alpha_1} \right)^{-\alpha_2}, \quad (4)$$

113 which is valid for both Φ_m and Φ_h . He noted that in order to obtain the correct physical
 114 behaviour for the gradients $\partial U / \partial z$ and $\partial \theta / \partial z$ in the free-convection limit ($z/L \rightarrow -\infty$), it
 115 is required that $\alpha_1 \alpha_2 = 1/3$. For this combination of values (4) behaves in this limit
 116 similarly to ‘classical’ free-convection expressions, with $\partial U / \partial z$ and $\partial \theta / \partial z$ varying
 117 proportionally to $z^{-4/3}$. He further noted that, for this choice of parameters, (1) - (2) may
 118 be integrated straightforwardly. Following W01 we will use $\kappa = 0.4$, $Pr_t = 0.95$, $\gamma_h =$
 119 7.86 , $\alpha_{1m} = \alpha_{1h} = 2/3$, $\alpha_{2m} = \alpha_{2h} = 1/2$ and $\gamma_m = 3.59$.

120 Subscripted indices s , n and fc hereafter denote values of flow parameters in the surface
 121 layer, in the neutral regime ($|L| \rightarrow \infty$), and in the free-convection regime ($|L| \rightarrow 0$),
 122 respectively.

123 The method developed here requires that z_{sfc} , u_{*fc} , L_{fc} , z_{sn} , u_{*n} and z_0 , be known in
 124 order to calculate $u_*(L)$ and $z_s(L)$. The primary input parameters are u_{*n} , z_{ifc} and the
 125 aerodynamic roughness height, z_0 , which must be provided initially.

126

127 2.3 Estimating parameters in the free-convection and neutral regimes

128 MOST shows good agreement with observations in regimes with sufficiently strong
 129 winds (high values of u_*) or under relatively low surface heat flux, $(\overline{w'\theta})_0$, where $|L| >$
 130 10^2 m. This theory is based on the assumption that, in the surface layer, z and L are the
 131 only relevant turbulence length scales. While this assumption is valid for relatively small
 132 values of $|z/L|$ (say $|z/L| < 1$), for larger values, in particular in the free-convection
 133 regime, MOST becomes incomplete. In the perfectly windless regime, purely dominated
 134 by thermal effects, both the mean wind speed and u_* approach zero, and MOST produces
 135 singularities and underestimates the surface fluxes. However, perfectly windless
 136 conditions occur very rarely, and the theory can still be applied, if conjugated with CBL
 137 theory, for low but non-zero winds, as will be shown below.

138 For the highly convective ABL, Deardorff (1970) suggested the following convective
 139 velocity scale

140
$$w_* = \left[\frac{g}{\theta_0} (\overline{w' \theta'})_0 z_{ifc} \right]^{1/3}. \quad (5)$$

141 The combination of MOST and Deardorff similarity theory, adopted here, provides a
 142 model that is consistent throughout the whole CBL (Kaimal et al. 1976) (hereafter K76),
 143 and for stabilities ranging from the neutral regime to the free-convection regime. This
 144 latter regime does not strictly correspond to $L = 0$, but rather to a minimum, suitably
 145 small value of $L = L_{fc}$, to be determined. In the free-convection regime we need to
 146 estimate z_{sfc} , u_{*fc} and L_{fc} . Given that u_{*fc} is defined in relation to w_* (as shown
 147 below), this latter quantity, defined by (5), must also be related to the known input
 148 parameters. This requires a total of four equations (see below).

149 Many observations have confirmed that the transition from the shear-driven turbulent
 150 regime of the surface layer to the buoyancy driven regime of the mixed layer usually
 151 occurs at a height of order $|L|$. Hence, in a highly-convective ABL (Garratt 1992),

152
$$z_{sfc} = c_{fc} |L_{fc}|, \quad (6)$$

153 where $c_{fc} = 2$. Equation 6 will be adopted hereafter in the free-convection regime.

154 Based on observations, Schumann (1988) (hereafter S88) assumed that $z_s/z_i = 0.1$. As
 155 will be seen later, this assumption is too restrictive over the whole stability interval,
 156 since, z_i is expected to increase and z_s to decrease as the stratification becomes more
 157 unstable. A more general definition of z_s is thus required. This is developed in Sect. 2.4.

158 Businger (1973) proposed the idea that u_* does not vanish at low wind speeds,
 159 introducing the concept of a ‘minimum friction velocity’, valid in the free-convection
 160 regime ($u_{*min} = u_{*fc}$). Combining (3) and (5) in this regime, we obtain

161
$$\frac{\kappa |L_{fc}|}{z_{ifc}} = \left(\frac{u_{*fc}}{w_*} \right)^3. \quad (7)$$

162 Using (6), it can be easily shown from (7) that z_{sfc}/z_{ifc} decreases as u_{*fc}/w_* decreases,
 163 which is physically plausible.

164 Various authors, such as S88 and Sykes et al. (1993) (hereafter S93), have advocated the
 165 view that u_{*fc}/w_* is a function of z_{sfc}/z_0 or z_{ifc}/z_0 as well. Following the less general
 166 relations derived by S88 and S93, valid only for limited intervals of z_0 , Zilitinkevich et

167 al. (2006) (hereafter Z06) suggested a more complete formulation for the relationship
 168 between u_{*fc}/w_* and z_{ifc}/z_0 , which takes into account the combined effects of
 169 buoyancy and shear forces,

$$170 \quad \frac{u_{*fc}}{w_*} = c_1 \left[\ln \frac{z_{ifc}/z_0}{(\ln z_{ifc}/z_0 - c_0)^3} + c_2 \right]^{-1} \quad \text{for } z_{ifc}/z_0 \geq \sigma, \quad (8)$$

$$171 \quad \frac{u_{*fc}}{w_*} = c_3 \left[\frac{z_0}{z_{ifc}} + c_4 \left(\frac{z_0}{z_{ifc}} \right)^{8/7} \right]^{1/6} \quad \text{for } z_{ifc}/z_0 < \sigma, \quad (9)$$

172 where $\sigma = 3.45 \times 10^5$, $u_{*fc}/w_*(\sigma) = 0.065$, $c_0 = 6.00$, $c_1 = 0.29$, $c_2 = -2.56$, $c_3 = 0.54$
 173 and $c_4 = 0.3$. Equations 8 and 9 agree very well with both LES and field data in the free-
 174 convection regime (Z06), and incorporate the best characteristics of the S88 and S93
 175 models.

176 The height z_i characterizes the PBL in a fairly integrated manner, being closely related to
 177 fundamental quantities such as $(\overline{w'\theta})_0$. For this reason, as a first approach, we suggest
 178 estimating the surface-layer scaling parameters in the free-convection regime based on a
 179 known value of z_{ifc} . This allows obtaining u_{*fc}/w_* directly from (8) - (9), since z_0 is
 180 also assumed to be known.

181 Our final constraint is based on Venkatram (1978) who, by using a simple mixed-layer
 182 model for the CBL, derived the following relationship between w_* and z_{ifc} ,

$$183 \quad w_* = c_5 z_{ifc}, \quad (10)$$

184 where $c_5 = 1.12 \times 10^{-3} \text{ s}^{-1}$. Equation 10 compares extremely well with observations (see
 185 Appendix 2). Using the available value of z_{ifc} , (10) allows us to determine w_* directly.

186 Equations 6 - 10 may thus be used to obtain the surface-layer parameters in the free-
 187 convection regime, as follows. Given z_{ifc} and z_0 , (8) or (9) is used to obtain u_{*fc}/w_*
 188 and (10) is used to obtain w_* , which yields u_{*fc} . Given z_{ifc} , w_* and u_{*fc} , determined in
 189 the preceding step, (7) is used to obtain L_{fc} . Finally, L_{fc} is inserted into (6) to obtain z_{sfc} .
 190 This yields u_{*fc} , L_{fc} and z_{sfc} , as required. Several different procedures analogous to the
 191 one just described would be possible, depending on what input parameters are known
 192 initially.

193 According to MOST, in the neutral regime

194
$$U_n(z) = \frac{u_{*n}}{\kappa} \ln\left(\frac{z}{z_0}\right). \quad (11)$$

195 Since, from (6), z_s is expected to depend on L , in the neutral regime at least (where no
196 stability effects exist), it seems reasonable to assume z_s to be a fixed fraction of z_i (Stull
197 1988),

198
$$z_{sn} = c_{sL} z_{in}, \quad (12)$$

199 where that fraction is conventionally defined as 5% to 10% of z_i (Stull 1988). In our
200 model, we assume $c_{sL} = 0.05$ (following Stull 2011). Here, and unlike what previous
201 authors have done, (12) is adopted only for the strictly neutral regime. As will be seen
202 later (Sect. 3.2), (12) holds approximately for a weakly unstable ABL, but not for a
203 strongly unstable ABL. In order to obtain z_{sn} from (12), it is still necessary to estimate
204 z_{in} . This can be done using the expression of Rossby and Montgomery (1935),

205
$$z_{in} = \frac{c_{zin} u_{*n}}{|f|}, \quad (13)$$

206 where $c_{zin} = 0.2$ (Garratt 1992).

207

208 2.4 Estimating z_s and u_* for arbitrary $L < 0$

209 The preceding section described the methodologies for estimating all the parameters
210 required for defining u_* and z_s in the free-convection and neutral regimes. Next we
211 explain the approach used to estimate these two parameters for arbitrary $L < 0$.

212 Since $|L|$ is the height at which the buoyant production of turbulence kinetic energy (E)
213 begins to dominate over shear production, the greater $(\overline{w'\theta'})_0$ is (i.e. the smaller $|L|$ is),
214 the bigger Δz_i and the smaller z_s become, because convectively-driven turbulence
215 increasingly dominates over shear-driven turbulence. So, there is a clear relationship
216 between z_s and $|L|$ (expressed by (6) in the strongly unstable regime). However, for
217 intermediate unstable regimes the dependence $z_s(L)$ is not known.

218 Based on the ABL model described in Sect. 2.1, we define z_s as the height where the
219 vertical derivative of $\theta(z)$ reaches a small prescribed fraction of its surface value. Using

220 this property, in the present model $z_s(L)$ is determined by (see details in Appendix 1)
 221 evaluating the root of,

$$222 \quad \frac{z_s}{z_{0\theta}} = \frac{1}{\alpha_{\psi_2}} \left(\frac{z_{0\theta}}{z_s} \right)^{-\alpha_{\psi_1}} \left[\frac{1 + \gamma_h (z_s/|L|)^{\alpha_1}}{1 + \gamma_h (z_{0\theta}/|L|)^{\alpha_1}} \right]^{-\alpha_2}, \quad (14)$$

223 for any value of L , assuming that $z_{0\theta}$, α_1 , α_2 , γ_h , α_{ψ_1} and α_{ψ_2} are provided. As (14)
 224 includes the influence on $z_s(L)$ of parameters in both extremes of the stability interval
 225 (see Appendix 1), it is expected to provide a good approximation over the whole stability
 226 range. As the roughness length for heat, $z_{0\theta}$, is not provided by C94, we use here z_0
 227 instead. Calculations not presented here show that the $z_s(L)$ dependences obtained using
 228 $z_{0\theta}/z_s$ or z_0/z_s are quite similar (the relation between $z_{0\theta}$ and z_0 assumed for this
 229 comparison follows Zilitinkevich 1995). Although $z_{0\theta}$ and z_0 differ, the proposed method
 230 for estimating z_s is not very sensitive to the exact value of z_0 as long as this is small.

231 $u_*(L)$, on the other hand, is calculated from

$$232 \quad u_*(z_s, L) = \kappa z_s \left[1 + \gamma_m \left(\frac{z_s}{|L|} \right)^{\alpha_1} \right]^{\alpha_2} \left(\frac{\partial U}{\partial z} \right)_{z_s}, \quad (15)$$

233 where, in accordance with the slab model adopted initially (see Sect. 2.1), it is expected
 234 that $\partial U/\partial z$ becomes small as $z \rightarrow z_s$. Here we assume that in (15) the shear $(\partial U/\partial z)_{z_s}$
 235 is constant, and, for convenience, equal to its neutral value. For $|L| \rightarrow \infty$ and at $z = z_s$,
 236 (1) reduces to $(\partial U/\partial z)_{z_{sn}} = u_{*n}/(\kappa z_{sn})$, in accordance with (11), where z_{sn} may be
 237 obtained from (12). The validity of the assumption $(\partial U/\partial z)_{z_s} = const.$ is tested in
 238 Appendix 2.

239 All quantities on the right-hand side of (15) are now known, and hence $u_*(z_s, L)$ may be
 240 determined in general. Finally, the $U(z)$ profile for the general unstably stratified case,
 241 which will be used in the HLR model for calculating $\Delta S(L)$,

$$242 \quad U(z) = \frac{u_*}{\kappa} \left\{ \ln \left(\frac{z}{z_0} \right) - 3 \ln \left[\frac{1 + \sqrt{1 + \gamma_m (z/|L|)^{2/3}}}{1 + \sqrt{1 + \gamma_m (z_0/|L|)^{2/3}}} \right] \right\}, \quad (16)$$

243 is obtained by integration of (1), using the velocity gradient expressed by (4) (see W01).

244 In the above treatment, it was assumed that the synoptic situation does not vary too
 245 rapidly compared with the time scales of flow over the ridge. Hence, according to MOST,
 246 the effect of L in the surface layer is dominant. As this quasi-steadiness is supported by
 247 the C94 campaign, the C94 observations can safely be used for testing the method
 248 proposed here. For more unsteady flows, it is likely necessary to use a time-dependent
 249 model for the whole ABL, such as that described by [Weng and Taylor \(2003\)](#), for
 250 providing upstream profiles $U(z)$ and $\theta(z)$ at different values of L . However, this
 251 approach would require more input parameters not available in the C94 observations, and
 252 their estimation would further increase the empiricism of the proposed method.
 253 Summarizing, in this section, assuming that z_0 , z_{sfc} , L_{fc} , z_{sn} and u_{*n} are known, we
 254 propose (14) and (15) for determining $z_s(L)$ and $u_*(L)$, respectively. $u_*(L)$ is then used
 255 in the HLR model to calculate $\Delta S(L)$ for flow over orography.

256

257 **3 Results and discussion**

258 The method presented above will be assessed using the observations of C94. These
 259 measurements were conducted during the Spring of 1984 and Summer of 1985, over
 260 Cooper's Ridge, located to the north-west of Goulburn, in New South Wales, Australia.
 261 This is a somewhat isolated north-south oriented, quasi-two-dimensional ridge of uniform
 262 low z_0 , located along a valley that forces the air to flow over the hill predominantly from
 263 the west side. The windward slope of the ridge (west side) can be well fitted using a
 264 simple bell-shaped profile $h(x) = h_0/\{1 + (x/a)^2\}$ (with $h_0 = 115$ m and $a = 400$ m).
 265 The lee side of the ridge falls away to about $0.5h_0$ before rising to another broader ridge.

266

267 3.1 Estimation of parameter values from the data

268 As mentioned in Sect. 2, for determining $z_s(L)$ and $u_*(L)$, the method developed here
 269 requires that z_0 , z_{sfc} , u_{*fc} , L_{fc} , z_{sn} and u_{*n} be known. From the data collected by C94,
 270 we have $u_{*n} = 0.35$ m s⁻¹, $z_0 = 0.05$ m and $f \approx 9 \times 10^{-5}$ s⁻¹. Using (13) we thus obtain z_{in}
 271 = 778 m, and using this value in (12) yields $z_{sn} = 39$ m.

272 The methodology described in Sect. 2.3 for estimating the flow parameters in the free-
 273 convection regime (z_{sfc} , u_{*fc} , L_{fc} and w_*) is now applied. As z_{ifc} is not supplied by
 274 C94, we will use a typical value corresponding to the season and latitude of the region

275 where the observations were taken. Figures containing the necessary information from
 276 ERA-40 Reanalysis, provided by [Von Engeln and Teixeira \(2013\)](#), suggest $z_{ifc} = 1550$
 277 m. Next, since $z_{ifc}/z_0 = 3 \times 10^4 < \sigma = 3.45 \times 10^5$, we must use (9) to calculate $u_{*fc}/w_* =$
 278 0.098. Substituting u_{*fc}/w_* and z_{ifc} into (7), we obtain $L_{fc} = -3.6$ m, and from (6) we
 279 obtain $z_{sfc} = 7.2$ m. Next, substitution of z_{ifc} in (10) gives $w_* = 1.74$ m s⁻¹, which in turn
 280 can be used for calculating u_{*fc} from $u_{*fc}/w_* = 0.098$, yielding $u_{*fc} = 0.17$ m s⁻¹. Table
 281 1 presents known and estimated parameters of the ABL in the free-convection regime,
 282 obtained by the present method and, for comparison, observations from runs 6A1 and
 283 6A2 of the field experiment reported by K76, corresponding to a highly convective ABL.
 284 As can be seen, the method proposed here seems to predict realistic results.
 285

Source	u_{*fc} (m s ⁻¹)	$ L_{fc} $ (m)	z_{sfc} (m)	z_{ifc} (m)	z_{sfc}/z_{ifc}	w_* (m s ⁻¹)	u_{*fc}/w_*
Present method	0.17	3.6	7.2	1550	0.005	1.70	0.098
Run 6A1	0.24	5.7	10.4	2095	0.005	2.43	0.099
Run 6A2	0.23	6.4	12.8	2035	0.006	2.21	0.104

286 **Table 1** Parameters of the ABL in the free-convection regime. Line 1: parameters used in the present
 287 method. Lines 2-3: similar parameters from runs 6A1 and 6A2 of the experiment described in [Kaimal et al.](#)
 288 (1976). The value of z_{sfc} for these runs was obtained from (6).
 289

290 It is interesting that, contrary to what happens in the neutral regime, the ratio $z_{sfc}/z_{ifc} =$
 291 0.005, estimated above, is significantly lower than the value assumed in (12). This value
 292 is of the same order of magnitude as those derived from the measurements of K76, taken
 293 in strongly convective conditions (see Table 1). As pointed out before, the smaller $|L|$ is,
 294 the more intense the turbulent mixing by large convective eddies in the mixed layer
 295 becomes, thereby reducing z_s . This corroborates, using real data, that the neutral
 296 approximation for z_{sn}/z_{in} cannot be considered realistic over the whole range of
 297 variation of L , particularly near the free-convection regime.
 298

299 3.2 Behaviour of z_s as a function of L

300 For a better understanding of the surface-layer structure, it is useful to define a transition
 301 height, z_{tr} , at which the convective contribution to $U(z)$ is as important as that of the

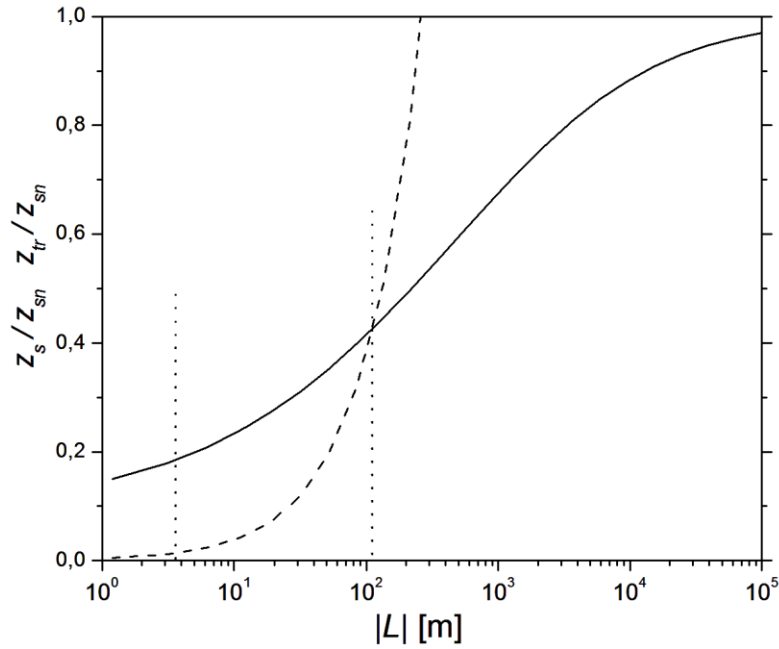
302 neutral log law. Following Kader and Yaglom (1990), from the W01 formulation (4), we
 303 can define

$$304 \quad z_{tr} = |L| \gamma_m^{-1/\alpha_1}. \quad (17)$$

305 It is expected that, in moderately to strongly unstable flow regimes $z_{tr} < z_s$, i.e. at the top
 306 of the surface layer $U(z)$ is no longer logarithmic.

307 Figure 1 presents the variation of z_s and z_{tr} , with $|L|$, normalized by z_{sn} . The solid line
 308 represents $z_s(L)$, computed using (14). In (14), the coefficients α_{ψ_1} and α_{ψ_2} , given by
 309 (23), take the values 0.415 and 0.018, respectively. $z_{tr}(L)$ (dashed line) is computed
 310 using (17).

311



312

313 **Fig 1** Surface-layer height, z_s , and transition height, z_{tr} , as a function of $|L|$, normalized by the surface-
 314 layer height for a neutral ABL, z_{sn} . Solid line: $z_s(L)$ obtained from (14), dashed line: $z_{tr}(L)$ obtained from
 315 (17). Vertical dotted lines: $|L_{fc}| = 3.6$ m (left), and $|L_{tr}| = 120$ m (right). $z_s(L)$ asymptotically approaches
 316 the constant values z_{sn} as $|L| \rightarrow \infty$ and $z_s(L) = 4.5$ m as $|L| \rightarrow 0$. $z_s(L_{fc}) = z_{sfc} = 7.2$ m (see Table 1).

317

318 The dotted vertical lines correspond to $|L_{fc}| = 3.6$ m (left) as determined previously (see
 319 Table 1), and the value of $|L_{tr}| = 120$ m (right) for which $z_s(L) = z_{tr}(L)$, i.e. for which
 320 the logarithmic and convective contributions to $U(z)$ are equally important. For $|L| > 400$
 321 m the logarithmic portion of $U(z)$ is overwhelmingly dominant compared to the

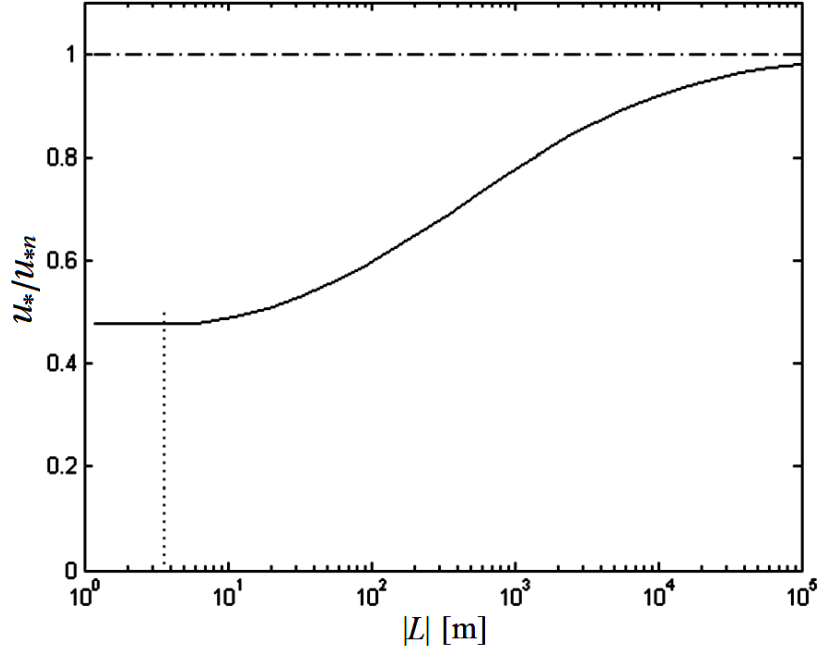
322 convective one, and therefore it can be considered that the ABL is in nearly neutral
323 conditions. For $L = L_{fc}$ or lower, the opposite is true, as the flow is nearly in free-
324 convection conditions. $z_s(L)$ physically behaves as expected, tending asymptotically to
325 constant values at each extreme of the stability interval (4.5 m as $|L| \rightarrow 0$, and z_{sn} for
326 $|L| \rightarrow \infty$). Figure 1 illustrates the way in which the surface layer becomes thinner with
327 increasing unstable stratification, because of the progressively higher buoyant production
328 of E in the mixed layer as $|L|$ decreases.

329

330 3.3 Behaviour of u_* as a function of L

331 Figure 2 presents u_* as a function of $|L|$, normalized by u_{*n} . The solid line corresponds
332 to $u_*(L)$ computed from (15), and the dash-dotted line extends the constant neutral value,
333 $u_{*n} = 0.35 \text{ m s}^{-1}$, over the whole stability interval, for comparison. Figure 2 shows that
334 $u_*(L)$ decreases with decreasing $|L|$ until it reaches its minimum value (u_{*min}) at $L =$
335 $|L_{min}|$. According to (15), for $|L| < |L_{min}|$, $u_*(L)$ would increase monotonically with
336 decreasing $|L|$, in such a way that $u_*(L) \rightarrow \infty$ for $|L| \rightarrow 0$. This behaviour occurs
337 because, as $|L| \rightarrow 0$, the term between brackets on the right-hand side of (15) tends to
338 infinity. This is a consequence of the physically unrealistic behaviour of MOST as $|L| \rightarrow$
339 0, producing singularities. For this reason, in Fig. 2 we have assumed that $u_*(L) = u_{*min}$,
340 for $|L| \leq |L_{min}|$.

341



342

343

344

345

346

347

Fig 2 Friction velocity (u_*) as a function of $|L|$, obtained from (15) (solid line) and constant u_* independent of the stability and equal to its value in the neutral regime ($u_{*n} = 0.35 \text{ m s}^{-1}$) (dash-dotted line). Both quantities are normalized by u_{*n} . The vertical dotted line indicates the value of L in the free-convection regime, $|L_{fc}| = 3.6 \text{ m}$ (see Table 1).

348

349

350

351

352

353

354

355

356

As can be seen in Fig. 2, $u_*(L)$ shows the expected physical behaviour (cf. Fig. 3.7 of Garratt 1992), approaching asymptotically (by design) u_{*n} as $|L| \rightarrow \infty$, and decreasing monotonically with decreasing $|L|$. However, the approach to u_{*n} as $|L| \rightarrow \infty$ is very gradual and u_* only takes a value mid-way between the neutral and free-convection limits for an $|L|$ of several hundred metres. Furthermore, the minimum value reached by $u_*(L)$ is $u_{*min} = 0.17 \text{ m s}^{-1}$ for $L_{min} = 3.4 \text{ m}$. Thus, $u_{*min} = u_{*fc}$ and $|L_{min}|$ almost coincides with $|L_{fc}| = 3.6 \text{ m}$, determined previously (see Table 1). This result further confirms that the assumption of constant $(\partial U / \partial z)_{z_s}$ is realistic, and allows obtaining reliable estimates of u_* over the whole stability interval.

357

358

359

360

361

Although u_{*fc} , is thus a minimum value of u_* , it is generally not as low compared with u_{*n} as might be expected. The case under consideration here, where $u_{*fc}/u_{*n} \approx 0.5$, which is not particularly low (see Sect. 3.1, Table 1), is a good example. This result ultimately suggests that a purely-thermal regime is unlikely (it was not realized in the C94 measurements, in particular). For these reasons, under nearly free-convection

362 conditions both u_{*fc} and L_{fc} differ substantially from zero, as is confirmed by the
363 observations of K76 (see Table 2), and further corroborated for a very unstable surface-
364 layer case by Steeneveld et al. (2005). This is what allows MOST to be used here for
365 describing a highly convective ABL.

366

367 3.4 Flow speed-up calculation

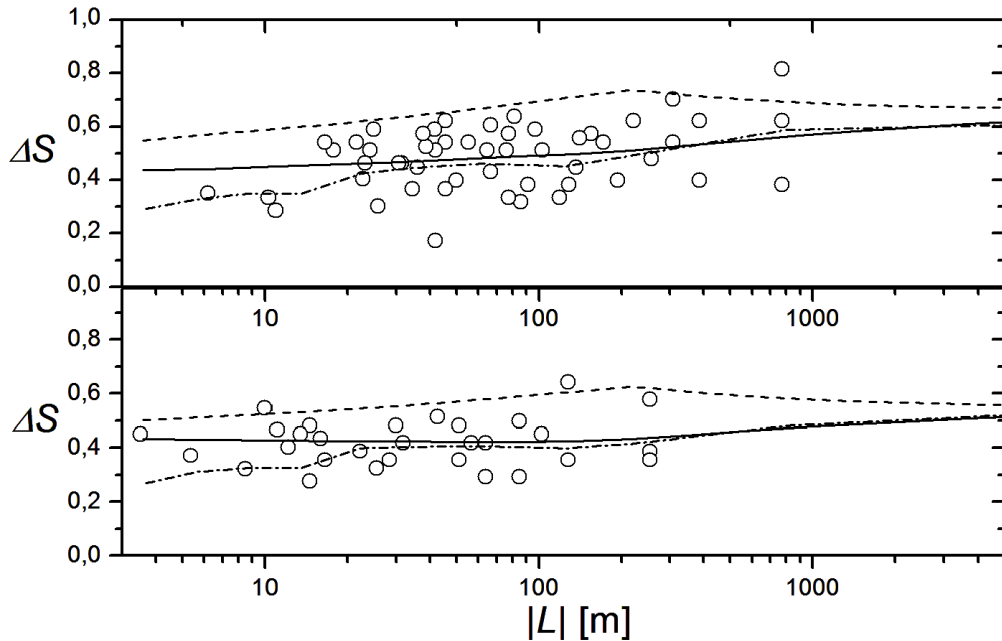
368 Since calculating $\Delta S(L)$ using the HLR model requires knowing $u_*(L)$, the main purpose
369 of this section is to use the behaviour of $\Delta S(L)$ predicted by that model to indirectly
370 assess the dependence on stability of $u_*(L)$ (and also of $z_s(L)$) established in the method
371 proposed here, by comparison with values of ΔS measured over a wide range of L by
372 C94, and simulated numerically using the FLEX model.

373 Suppose that at a hilly location $\Delta S(L)$ needs to be estimated, assuming that the only
374 available parameters are z_0 and the mean wind speed, $U(z)$, measured at a suitably low
375 height such that, according to MOST, (11) is approximately valid for any L . Equation 11
376 can then be used for estimating u_{*n} . Once z_0 and u_{*n} are known, the present method
377 allows systematically obtaining $z_s(L)$, then $u_*(L)$ and finally $\Delta S(L)$, for the whole
378 unstable stratification parameter range.

379 In the specific case under consideration here, first using as input parameters $u_{*n} = 0.35$ m
380 s^{-1} and $z_0 = 0.05$ m (from C94), $u_*(L)$ is calculated using the proposed method. Next, this
381 $u_*(L)$ is used in the HLR model applied to flow over Cooper's ridge to calculate $\Delta S(L)$.
382 $\Delta S(L)$ is also calculated assuming that $u_* = const. = u_{*n}$, regardless of the observed L .
383 This simpler choice, often used for estimating $\Delta S(L)$ in flow over orography (e.g. W97),
384 is what the present approach aims to improve. Finally, the ΔS values are compared, for a
385 range of L , between the HLR model, the C94 measurements, and the FLEX model.

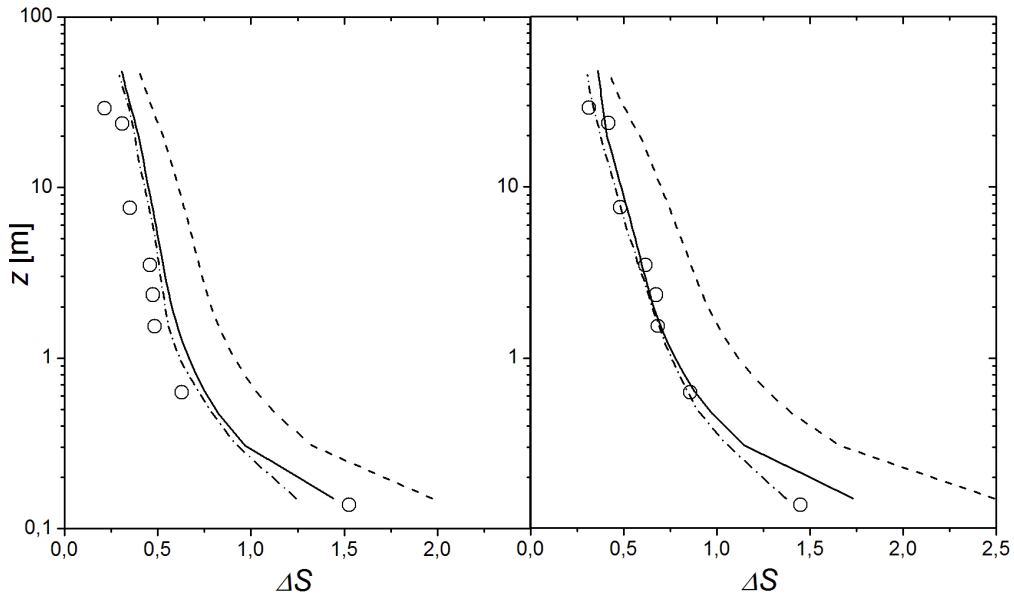
386 For the sake of simplicity the HLR and FLEX models are not described in detail here. A
387 brief description of the HLR model can be found in W97 or A09. FLEX is a microscale-
388 mesoscale, nonlinear and non-hydrostatic model, which was developed and validated
389 against experimental and field data by Argaín (2003) and A09. This model has been
390 tested and used extensively, namely by Teixeira et al. (2012, 2013a, 2013b) for assessing
391 analytical mountain wave drag predictions in 2D flows by comparison with numerical
392 simulations.

393 All the numerical simulations presented here used a main grid of (160×364) points for a
 394 domain of (8000×2000) m size. The horizontal domain extent is $20a$ ($7a$ upstream of
 395 the ridge maximum and $13a$ downstream). From $z = 40$ m downward the level of grid
 396 refinement is gradually increased, and the lowest level is at a similar distance to the
 397 surface as the observations (≈ 0.15 m). At the surface a no-slip condition is used, and
 398 $(\overline{w'\theta'})_0$ and other turbulent quantities (turbulent kinetic energy, E , and dissipation ε of
 399 E), are specified, for each L , by assuming that viscous dissipation balances shear and
 400 buoyancy production. At the upper boundary, constant U and θ are prescribed, and L and
 401 the derivatives of E and ε are set to zero.
 402 Observations, and both theoretical and numerical predictions of ΔS as a function of $|L|$
 403 are shown in Fig. 3, at $z = 8$ m and $z = 16$ m. The HLR model is applied in two cases: a)
 404 $u_* = u_{*n}$, regardless of $|L|$ (dashed line), and b) the friction velocity is calculated for each
 405 $|L|$, using the method proposed here (15) (solid line).
 406



407
 408 **Fig 3** Variation of the fractional speed-up (ΔS) as a function of stability, above the hill crest, at the heights
 409 $z = 8$ m (top) and $z = 16$ m (bottom). Solid line: u_* computed using (15); dotted line: u_* kept constant,
 410 regardless of the stability, and equal to the neutral ABL value ($u_{*n} = 0.35 \text{ m s}^{-1}$); dash-dotted line: FLEX
 411 model; symbols: observations from C94.
 412

413 The significant differences between the ΔS curves, obtained using the two different
 414 definitions of u_* , reveals that ΔS is very sensitive to the dependence of u_* on $|L|$, as
 415 shown by A09 for the stable case. The results assuming $u_* = u_{*n}$ (dashed lines)
 416 overestimate the observations considerably. In both panels of Fig. 3, the improvement in
 417 the performance of the theoretical model, owing to the new method of calculating u_*
 418 (solid lines), is significant over the whole stability interval. In general, this new method
 419 produces results much closer to both the field measurements (despite the considerable
 420 scatter in the data) and the numerical simulation results. ΔS calculated from the
 421 theoretical model with u_* depending on L has a rather flat variation with $|L|$, especially at
 422 $z = 16$ m, and although decreasing more substantially with $|L|$ at $z = 8$ m, slightly
 423 overestimates both the measurements and the numerical simulations for the lowest values
 424 of $|L|$.
 425



426
 427 **Fig 4** Profiles of the fractional speed-up ratio (ΔS) above the hill crest, for $|L| = 33$ m (left) and $|L| = 222$ m
 428 (right). Solid line: u_* computed using (15); dashed line: u_* kept constant at $u_{*n} = 0.35$ m s⁻¹; dash-dotted
 429 line: FLEX model; symbols: observations from C94.

430
 431 Profiles of observations (C94), and both theoretical and numerical predictions of ΔS
 432 directly above the hill crest, for $|L| = 33$ m (left panel) and $|L| = 222$ m (right panel) are
 433 shown in Fig. 4. $|L| = 33$ m and $|L| = 222$ m correspond to strong and moderately weak

434 unstable stratification, respectively. In both cases, the proposed method compares better
435 both with the numerical model and with the field data, although it slightly overestimates
436 the observations in the more unstable case. Nevertheless, a general decrease of ΔS as one
437 shifts from the higher to the lower $|L|$ value is qualitatively reproduced. Given the
438 precision of the measurements and flow assumptions, not too much importance should be
439 attached to this overestimate, which also occurs in the numerical simulations
440 (consistently, a similar discrepancy can be detected for the theoretical model on the far
441 left of Fig. 3 at $z = 8$ m).

442 ΔS is much more severely overestimated, in both cases, by the profiles with a prescribed
443 constant $u_* = u_{*n}$, due essentially to the significant fractional deviation between u_{*n} and
444 the more accurate value of u_* determined from (15). This fractional deviation amounts to
445 $\sim 45\%$ for $|L| = 33$ m and to $\sim 35\%$ for $|L| = 222$ m (see Fig. 2), but this does not translate
446 into proportional deviations for ΔS , as the value of ΔS , where u_* is calculated from (15),
447 actually becomes closer to that where $u_* = u_{*n}$ as $|L|$ decreases (see Fig. 3). The fact that
448 there is such a large difference in the results using $u_*(L)$ and $u_* = u_{*n}$ for the weakly
449 unstable case might seem suspect, but Fig. 2 explains it, since for $|L| = 222$ m, $u_*(L)$ still
450 differs very substantially from u_{*n} .

451 It should be pointed out that at the lowest measurement level, ΔS should depend very
452 weakly on L , because near enough to the ground the flow is always approximately
453 neutral. The overestimate of the measured ΔS at that level by the theoretical model for $|L|$
454 $= 222$ m can probably be attributed to an inherent bias of the HLR solution, noted by
455 W97 and A09.

456

457 **4 Summary and conclusions**

458 In this paper, we propose a new method for estimating two scaling parameters of the
459 ABL: the surface-layer height z_s and the friction velocity u_* , as a function of stability
460 (quantified by the Obukhov length scale L), for an unstable ABL. These two parameters
461 are important for characterizing the unstable ABL, in particular its coupling with the
462 overlying convective mixed layer. Moreover, a correct estimation of u_* , whose
463 dependence on L is often not accounted for in a physically consistent way, is crucial for

464 producing accurate predictions of the speed-up (ΔS) in flow over hills, which is relevant
465 for a number of engineering applications.

466 Using a physical approach that is developed specifically for unstable conditions, via a
467 combination of MOST and convective mixed-layer scaling, our model takes into account
468 the fact that z_s decreases as the unstable stratification becomes stronger, due to erosion of
469 the surface-layer eddies by more energetic buoyancy-dominated eddies from the
470 convective mixed layer. The model also takes into account the fact that u_* decreases as
471 the ABL becomes more unstable, attaining a minimum value, but does not, in general,
472 approach zero in the free-convection limit, unless the wind vanishes completely (in which
473 case the concept of ΔS loses its meaning). The variation of u_* affects the turbulent fluxes
474 of various properties, and consequently the mean profiles of those properties, including
475 the wind speed $U(z)$, which determines the behaviour of ΔS .

476 Procedures to obtain boundary-layer parameters in the neutral and free-convection
477 regimes, and for bridging across these regimes, to cover the complete unstable ABL
478 parameter range, were developed and tested using available field data. The performance
479 of the model was then evaluated more comprehensively, by comparing predictions of ΔS
480 in unstable conditions, using the linear model of HLR incorporating the new friction
481 velocity formulation, against measurements from C94, and numerical simulations of the
482 FLEX mesoscale-microscale model. Agreement was found to be substantially improved
483 relative to results where u_* is held constant. This emphasizes the importance of
484 accounting for the full dynamics of the unstable ABL, including the variation of u_* and z_s
485 with stability, for correctly estimating ΔS . The proposed method, whose possible
486 applications are not limited to improving the calculation of ΔS , should be seen as a
487 preliminary step in the development of better tools for the parametrization of unstable
488 ABLs. Further validation of this method by comparison with observations remains
489 necessary.

490

491 **Acknowledgements** The authors thank two anonymous referees and the co-editors for insightful
492 comments, which substantially improved this article. M.A.C.T. acknowledges the financial support of the
493 European Commission, under Marie Curie Career Integration Grant GLIMFLO, contract PCIG13-GA-
494 2013-618016. P.M.A.M. acknowledges the financial support of FCT, under Grant RECI/GEO-
495 MET/0380/2012.

496

497 **Appendix 1. Accuracy of the $(\partial\theta/\partial z)_{z_s} = \text{const.}$ approximation**

498 In the present model, the form of $z_s(L)$ is established using the temperature gradient
 499 $\partial\theta/\partial z$, which can be obtained from (2) and (4), yielding

500
$$\frac{\partial\theta}{\partial z} = \theta_*' \left[1 + \gamma_h \left(\frac{z}{|L|} \right)^{\alpha_1} \right]^{-\alpha_2} z^{-1}, \quad (18)$$

501 where $\theta_*' = Pr_t \theta_* / \kappa$. According to (18), $\partial\theta/\partial z \rightarrow 0$ as $z \rightarrow \infty$. This is consistent with
 502 the assumption that $\theta = \text{const.}$ in the mixed layer, so, at $z = z_s$ the derivative $(\partial\theta/\partial z)_{z_s}$
 503 should be suitably small, and this smallness is exploited to obtain z_s . Note that a similar
 504 condition could be based on the mean velocity gradient (1), but we think that $\theta = \text{const.}$
 505 is more reliable in the mixed layer, since $U(z)$ profiles may exhibit non-negligible shear
 506 above the surface layer, due to variation of the pressure perturbation induced by the
 507 orography with height or the Coriolis force. Taking this into account, the ratio

508
$$\Psi(z_s, L) = \frac{(\partial\theta/\partial z)_{z_s}}{(\partial\theta/\partial z)_{z_{0\theta}}} = \left[\frac{1 + \gamma_h (z_s/|L|)^{\alpha_1}}{1 + \gamma_h (z_{0\theta}/|L|)^{\alpha_1}} \right]^{-\alpha_2} \frac{z_{0\theta}}{z_s}, \quad (19)$$

509 implicitly determines $z_s(L)$, if the form of the function $\Psi(z_s, L)$ is known. In (19)
 510 $(\partial\theta/\partial z)_{z_s}$ and $(\partial\theta/\partial z)_{z_{0\theta}}$ are obtained by evaluating (18) at z_s and the temperature
 511 roughness height, $z_{0\theta}$, respectively. As defined by (19), $\Psi(z_s, L)$ varies monotonically
 512 from 1 to zero as $z_{0\theta}/z_s$ decreases. Moreover, $\Psi(z_s, L)$ depends only weakly on L : by
 513 substituting L_{fc} , z_{sfc} , z_{sn} and $L_n = \infty$ (see Sect. 3.1, Table 1) into (19) we may calculate
 514 the ratio $\Gamma = \Psi(z_{sn}, L \rightarrow -\infty) / \Psi(z_{sfc}, L_{fc}) \approx 0.6$, which is of order 1.

515 The limits of $\Psi(z_s, L)$ at the theoretical extremes of the stability interval are, respectively,

516
$$\Psi_{sfc} = \Psi(z_{sfc}, L \rightarrow 0) = \lim_{|L| \rightarrow 0} \Psi(L) = \left(\frac{z_{0\theta}}{z_{sfc}} \right)^{\alpha_1 \alpha_2 + 1}, \quad (20)$$

517
$$\Psi_{sn} = \Psi(z_{sn}, L \rightarrow \infty) = \lim_{|L| \rightarrow \infty} \Psi(L) = \frac{z_{0\theta}}{z_{sn}}. \quad (21)$$

518 For both strongly and weakly unstable flows, (20) - (21) suggest that $\Psi(z_s, L) \propto (z_{0\theta}/$
 519 $z_s)^\alpha$, where α is a dimensionless constant. Taking this result into account, we

520 hypothesize that this form holds for the whole stability interval, yielding the following
 521 approximate definition for $\psi(z_s, L)$,

$$522 \quad \Psi(z_s, L) = \alpha_{\psi_2} \left(\frac{z_{0\theta}}{z_s} \right)^{\alpha_{\psi_1}}, \quad (22)$$

523 where α_{ψ_1} and α_{ψ_2} are dimensionless constants. These two constants can be determined
 524 by taking the limits of (22) in the free-convection and neutral regimes, and comparing the
 525 corresponding expressions with (20) and (21), respectively. This produces a set of two
 526 equations, which may be solved for α_{ψ_1} and α_{ψ_2} , yielding

$$527 \quad \alpha_{\psi_1} = \ln \left[\frac{\Psi(z_{sn}, L \rightarrow \infty)}{\Psi(z_{sfc}, L_{fc})} \right] / \ln \left(\frac{z_{sfc}}{z_{sn}} \right) \quad \alpha_{\psi_2} = \Psi(z_{sfc}, L_{fc}) \left(\frac{z_{0\theta}}{z_{sfc}} \right)^{-\alpha_{\psi_1}} \quad (23)$$

528 By combining (19) and (22), (14) is obtained.

529

530 Appendix 2. Accuracy of the $(\partial U / \partial z)_{z_s} = \text{const.}$ approximation

531 Here we show that the approximation $(\partial U / \partial z)_{z_s} = \text{const.}$, used in Sect. 2.4 for
 532 evaluating u_* , is supported by measurements. Let us consider the following ratio, by
 533 using MOST,

$$534 \quad \beta_{MOST} = \frac{(\partial U / \partial z)_{z_{sn}}}{(\partial U / \partial z)_{z_{sfc}}} = \frac{c_{fc} \beta_1 |f|}{\underbrace{c_{SL} c_{zin}}_{\alpha_5}} \frac{|L_{fc}|}{u_{*fc}}, \quad (24)$$

535 where $\beta_1 = (1 + \gamma_m c_{fc}^{\alpha_1})^{\alpha_2}$. Equation 24 is obtained by combining (1), (4), (6), (12) and
 536 (13). Using parameters from C94 (see Sect. 3.1) we obtain $\alpha_5 = 0.0466 \text{ s}^{-1}$. For the values
 537 of L_{fc} and u_{*fc} shown in Table 1, this yields $\beta_{MOST} = 0.99$. The remarkable closeness of
 538 this value to 1 is fortuitous, although it obviously depends on the values adopted for c_{zin} ,
 539 c_{fc} and c_{SL} . For checking further the approximation $\beta_{MOST} \approx 1$ we use the K76
 540 observations (keeping the same α_5), which were carried out in a daytime well-mixed
 541 CBL, with evidence of significant heat and momentum entrainment through the capping
 542 inversion.

543

Run	u_{*fc} (m s ⁻¹)	$ L_{fc} $ (m)	z_{ifc} (m)	w_* (m s ⁻¹)	w_*/z_{ifc} (s ⁻¹)	β_{MOST}
6A1	0.24	5.7	2095	2.43	1.16×10^{-3}	1.1

6A2	0.23	6.4	2035	2.21	1.09×10^{-3}	1.3
-----	------	-----	------	------	-----------------------	-----

544 **Table 2** CBL parameters measured by [Kaimal et al. \(1976\)](#). Columns 6 and 7 show, respectively, w_*/z_{ifc} ,
545 and β_{MOST} , calculated from the data (the second quantity by using (24)).

546

547 **Table 2** shows CBL parameters obtained by K76, corresponding to the runs with the
548 smallest values of $|L|$, typical of nearly free-convection regimes. As can be seen, the
549 values of β_{MOST} are close to 1, corroborating the hypothesis $\beta_{MOST} \approx 1$. Moreover,
550 column 6 supports (10), proposed by [Venkatram \(1978\)](#), since $c_5 = w_*/z_{ifc}$ varies within
551 a narrow range. [Venkatram \(1978\)](#) estimated $c_5 = 1.12 \times 10^{-3} \text{ s}^{-1}$, which is quite close to
552 both values shown in **Table 2**. Therefore, the assumption that c_5 is a constant is plausible.
553 If the assumption $\beta_{MOST} = 1$ is accepted, (24) defines a relationship between α_5 , $|L_{fc}|$ and
554 u_{*fc} . If parameters c_{fc} and c_{zin} are assumed to be non-adjustable, this is equivalent to a
555 relation between $|L_{fc}|$, u_{*fc} and c_{SL} . Equation 13 is only applicable if $|L| \rightarrow \infty$ (a rarely
556 observed situation), so the parameter c_{zin} may have a considerable uncertainty.
557 [Zilitinkevich et al. \(2012\)](#) and [Garratt \(1992\)](#) discuss this topic at length. It would be
558 interesting to explore the constraint defined by (24) further to develop relations other than
559 (13) for estimating z_{in} , but that is beyond the scope of the present paper.

560 We also carried out a similar analysis using the classical free-convection formulation of
561 [Prandtl \(1932\)](#) for the mean velocity gradient,

$$562 \quad \left(\frac{\partial U}{\partial z} \right)_{z_{sfc}} = \frac{c_u u_{*fc} (\kappa |L_{fc}|)^{1/3}}{z_{sfc}^{4/3}} = \frac{c_u \kappa^{1/3} u_{*fc}}{c_{fc}^{4/3} |L_{fc}|}, \quad (25)$$

563 where $c_u = 1.7$. In this case we would obtain a ratio $(\partial U/\partial z)_{z_{sfc}}/(\partial U/\partial z)_{z_{sn}}$ with a
564 similar parameter dependence as (24) and $\alpha_5 = 0.0453 \text{ s}^{-1}$. The proximity between the
565 values of α_5 obtained using both formulations for $(\partial U/\partial z)_{z_{sfc}}$ confirms that the MOST
566 formulation adopted here is physically consistent, hence it may be used to describe the
567 free-convection regime.

568

569 **References**

570 [Argaín JL \(2003\)](#) Modelação de Escoamentos Atmosféricos: Efeitos Orográficos e de Camada Limite (in
571 Portuguese). Ph.D. Thesis, Universidade do Algarve, 275 pp

572 Argañ JL, Miranda PMA, Teixeira MAC (2009) Estimation of the friction velocity in stably stratified
573 boundary-layer flows over hills. *Boundary-Layer Meteorol* 130: 15-28

574 Businger JA (1973) A Note on Free Convection. *Boundary-Layer Meteorol* 4: 323–326

575 Coppin PA, Bradley EF, Finnigan JJ (1994) Measurements of flow over an elongated ridge and its thermal
576 stability dependence: The mean field. *Boundary-Layer Meteorol* 69: 173-199

577 Deardorff JW (1970) Convective velocity and temperature-scales for the unstable planetary boundary layer.
578 *J Atmos Sci* 27: 1211–1213

579 Garratt JR (1992) *The Atmospheric Boundary Layer*, Cambridge University Press, 316 pp

580 Hunt JCR, Leibovich SL, Richards KJ (1988) Turbulent Shear Flows Over Low Hills. *Q J R Meteorol Soc*
581 29: 16-26

582 Kader BA, Yaglom AM (1990), Mean Fields and Fluctuation Moments in Unstably Stratified Turbulent
583 Boundary Layers, *J Fluid Mech* 212: 637–662

584 Kaimal JC, Wyngaard JC, Haugen DA, Cote OR, Izumi Y, Caughey SJ, Readings CJ (1976) Turbulence
585 Structure in the Convective Boundary Layer. *J Atmos Sci* 33: 2152-2169

586 McNaughton KG (2004) Turbulence Structure of the Unstable Atmospheric Surface Layer and Transition
587 to the Outer Layer. *Boundary-Layer Meteorol* 112: 199-221

588 Prandtl L (1932) *Meteorologische Anwendungen der Strömungslehre*. *Beitr Phys Fr Atmos* 19: 188-202

589 Rossby CG, Montgomery RB (1935) The layers of frictional influence in wind and ocean currents. *Pap*
590 *Phys Oceanogr Meteorol* 3: 101 pp

591 Schumann U (1988) Minimum Friction Velocity and Heat Transfer in the Rough Surface Layer of a
592 Convective Boundary Layer. *Boundary-Layer Meteorol* 44: 311–326

593 Steeneveld GJ, Holtslag AAM, DeBruin HAR (2005) Fluxes and gradients in the convective surface layer
594 and the possible role of boundary-layer depth and entrainment flux, *Boundary-Layer Meteorol* 116:
595 237-252

596 Stull, RB (1988) *An Introduction to Boundary-Layer Meteorology*, Kluwer Academic Publishers,
597 Dordrecht,, 670 pp

598 Stull, RB (2011) *Meteorology for Scientists and Engineers*, 3rd edition, University of British Columbia,
599 Vancouver British Columbia, 938 pp

600 Sykes RI, Henn DS, Lewellen WS (1993) Surface-layer description under free-convection conditions. *Q J*
601 *R Meteorol Soc* 119: 409–421

602 Teixeira MAC, Argañ JL, Miranda PMA (2012) The importance of friction in mountain wave drag
603 amplification by Scorer parameter resonance. *Q J R Meteorol Soc* 138: 1325-1337

604 Teixeira MAC, Argañ JL, Miranda PMA (2013a) Drag produced by trapped lee waves and propagating
605 mountain waves in a two-layer atmosphere. *Q J R Meteorol Soc* 139: 964-981

606 Teixeira MAC, Argañ JL, Miranda PMA (2013b) Orographic drag associated with lee waves trapped at an
607 inversion. *J Atmos Sci* 70: 2930–2947

608 Venkatram A (1978) Estimating the convective velocity scale for diffusion applications. *Boundary-Layer*
609 *Meteorol* 15: 447-452

610 Von Engeln A and Teixeira J (2013) A planetary boundary-layer height climatology derived from ECMWF
611 re-analysis data. *J. Clim* 26: 6575–6590

612 Weng W (1997) Stably stratified boundary-layer flow over low hills: A comparison of model results and
613 field data. *Boundary-Layer Meteorol* 85: 223-241

614 Weng W, Taylor PA (2003) On modelling the one-dimensional atmospheric boundary layer. *Boundary-*
615 *Layer Meteorol.*, 107:371-400

616 Wilson DK (2001) An Alternative Function for the Wind and Temperature Gradients in Unstable Surface
617 Layers. *Boundary-Layer Meteorol* 99: 151–158

618 Zilitinkevich SS (1995) Non-local turbulent transport: Pollution dispersion aspects of coherent structure of
619 convective flows. *Air Pollution Theory and Simulation*. Power H, Moussiopoulos N, Brebbia CA, Eds.,
620 Vol. I, *Air Pollution III*, Computational Mechanics Publications, 53–60.

621 Zilitinkevich SS, Hunt JCR, Grachev AA, Esau IN, Lalas DP, Akylas E, Tombrou M, Fairall CW,
622 Fernando HJS, Baklanov AA, Joffre SM (2006) The influence of large convective eddies on the
623 surface-layer turbulence. *Q J R Meteorol Soc* 132: 1423-1456

624 Zilitinkevich SS, Tyuryakov SA, Troitskaya YI, Mareev EA (2012) Theoretical Models of the Height of
625 the Atmospheric Boundary Layer and Turbulent Entrainment at Its Upper Boundary. *Izvestiya,*
626 *Atmospheric and Oceanic Physics* 48(1): 133-142